

How contact metamorphism can trigger global climate changes: Modeling gas generation around igneous sills in sedimentary basins

Ingrid Aarnes^{a,*}, Henrik Svensen^a, James A.D. Connolly^b, Yuri Y. Podladchikov^a

^a *Physics of Geological Processes (PGP), Department of Physics, University of Oslo, P.O. Box 1048 Blindern, Norway*

^b *Department of Earth Sciences, ETH Zürich, Clausiusstrasse 25, 8092 Zürich, Switzerland*

Received 21 July 2009; accepted in revised form 7 September 2010; available online 17 September 2010

Abstract

Large volumes of greenhouse gases such as CH₄ and CO₂ form by contact metamorphism of organic-rich sediments in aureoles around sill intrusions in sedimentary basins. Thermogenic gas generation and dehydration reactions in shale are treated numerically in order to quantify basin-scale devolatilization. We show that aureole thicknesses, defined as the zone of elevated metamorphism relative to the background level, vary within 30–250% of the sill thickness, depending on the temperature of the host-rock and intrusion, besides the sill thickness. In shales with total organic carbon content of >5 wt.%, CH₄ is the dominant volatile (85–135 kg/m³) generated through organic cracking, relative to H₂O-generation from dehydration reactions (30–110 kg/m³). Even using conservative estimates of melt volumes, extrapolation of our results to the scale of sill complexes in a sedimentary basin indicates that devolatilization can have generated ~2700–16200 Gt CH₄ in the Karoo Basin (South Africa), and ~600–3500 Gt CH₄ in the Vøring and Møre basins (offshore Norway). The generation of volatiles is occurring on a time-scale of 10–1000 years within an aureole of a single sill, which makes the rate of sill emplacement the time-constraining factor on a basin-scale. This study demonstrates that thousands of gigatons of potent greenhouse gases like methane can be generated during emplacement of Large Igneous Provinces in sedimentary basins.

© 2010 Elsevier Ltd. All rights reserved.

1. INTRODUCTION

The emplacement of Large Igneous Provinces (LIPs) were synchronous with major climatic and environmental perturbations since the Paleozoic (e.g. Stothers, 1993; Wignall, 2001; Courtillot and Renne, 2003). LIPs are made up by an extensive network of sills and dikes emplaced into sedimentary basins, in addition to the large volumes of flood basalts. Pronounced negative carbon-isotope ($\delta^{13}\text{C}$) excursions are identified from proxy data records covering these events, which can be explained by a release of ¹²C-enriched carbon gases to the atmosphere (e.g. Jenkyns, 1988; Dickens et al., 1995; Hesselbo et al., 2000). The sources of these gases are debated, and both gas hydrate dissociation

and lava degassing have been suggested. Svensen et al. (2004) suggested that the source of carbon could be contact metamorphism of organic-rich shale around intrusive sills during LIP emplacement, and that the generated aureole gases subsequently vented to the atmosphere.

The hypothesis of thermogenic gas generation during contact metamorphism is supported by the presence of more than 1000 degassing pipes up to 150 m in diameter, originating at sill aureoles (Planke et al., 2005; Svensen et al., 2007). The hypothesis is now adopted to explain the end-Guadalupian (261 Ma), the end-Permian (252 Ma), the end-Triassic (200 Ma), the Toarcian (183 Ma), and the Paleocene-Eocene Thermal Maximum (PETM) (55 Ma) (Payne and Kump, 2007; Svensen et al., 2007, 2009; Retallack and Jahren, 2008). The key process of this hypothesis, gas generation during contact metamorphism of organic matter, remains poorly constrained.

* Corresponding author. Tel.: +47 97960192.

E-mail address: ingrid.aarnes@fys.uio.no (I. Aarnes).

Organic matter stored in sedimentary rocks (e.g. black shale) represents one of the Earth's largest carbon reservoirs (Falkowski et al., 2000). This reservoir is tapped during contact metamorphism of organic material (e.g. Perregaard and Schiener, 1979; Saxby and Stephenson, 1987; Othman et al., 2001). Carbon loss in aureoles is manifest by a decreasing total organic carbon (TOC) content and increasing vitrinite reflectance (%Ro) towards the contact with intrusions.

The aim of this study is to quantify gas formation by cracking of organic material and devolatilization of minerals in contact aureoles by numerical modeling (Fig. 1b). We quantify aureole thickness on the basis of vitrinite reflectance profiles and obtain the mass and composition of devolatilization products as a function of sill volume and TOC content (Fig. 1c). The composition and fate of the generated fluids are discussed. We extrapolate our results from aureole-scale (10–100 m above and below an intrusion) to basin-scale (>80,000 km² of intruded area) to evaluate the gas generation potential from contact metamorphism during LIP formation and compare it to the global carbon cycle perturbations.

2. AUREOLE PROCESSES

2.1. Contact metamorphism of organic material

Maturation of organic material in contact with igneous intrusions is thoroughly documented in the literature (Table 1) using several methods, including vitrinite reflectance measurements, Rock-Eval pyrolysis, gas chromatography, and stable isotope analysis (e.g. Powers and Clapp, 1932; Saxby and Stephenson, 1987; George, 1992). Contact metamorphism of organic material leads to elevated vitrinite reflectance (%Ro), loss of TOC, increased aromatization and changes in carbon isotope compositions ($\delta^{13}\text{C}$) of the residual organic material towards the contact (e.g. Clayton and Bostick, 1986; Barker and Bone, 1995; Meyers and

Simoneit, 1999). Sill intrusions are accordingly potentially important in many sedimentary basins for maturing source rocks and producing methane-rich gases.

Many studies focus on local contact metamorphic effects, and sill thicknesses, host-rock compositions, and depth of emplacement vary considerably. We have summarized 36 aureole case studies around sheet intrusions published since 1959 (Table 1) to get an overview of published data and aureole processes that have been considered in the literature.

A key issue discussed in the literature is the contact aureole thickness, defined as the zone of elevated metamorphism relative to the background level, starting at the intrusion contact. A common way of estimating the aureole thickness is based on vitrinite reflectance profiles, and for the numerical simulations we define the aureole thickness as the zone within $\geq 1\%$ Ro. The aureole thicknesses usually vary between 30% and 200% of the intrusion thickness (Table 1). The great span in this parameter in published aureole data suggests an influence of several factors, for example degree of background maturation, varying temperature of intrusion contact, different fluid systems, or multiple intrusions (e.g. Raymond and Murchison, 1988; Barker et al., 1998; Kjeldstad et al., 2003). To constrain some of these variations and how they influence the aureole processes, we test how key parameters (intrusion temperature, host-rock temperature and sill thickness) affect both the aureole thickness and the mass of generated gases during heating. Through numerical modeling we are able to cover the whole range of natural variations in intrusion thicknesses and temperature history, and simulate the response of the host shale.

2.2. Contact metamorphism of inorganic material

Contact metamorphic processes, such as mineral dehydration, decarbonation and host-rock melting reactions are commonly done in aureoles of large plutons (e.g. Jamtveit et al., 1992; Svensen and Jamtveit, 1998; Holness and

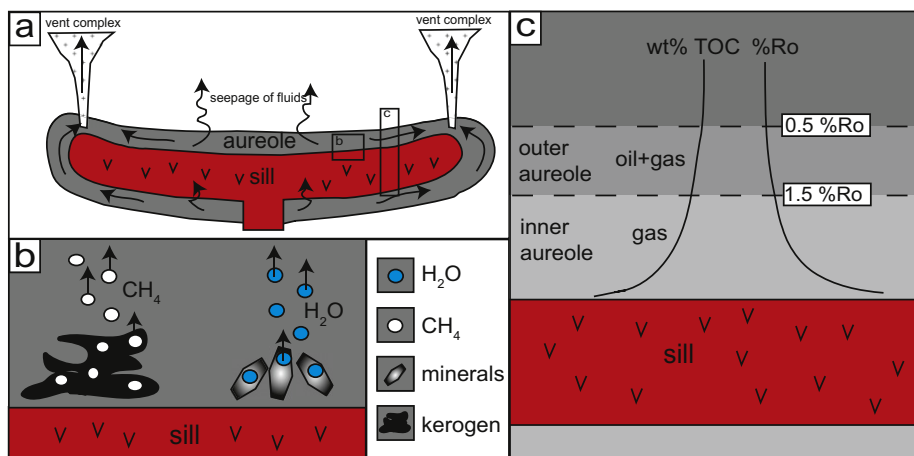


Fig. 1. (a) Schematic model of a contact aureole around a sill intrusion emplaced into sedimentary rocks. Overpressure in the aureole may ultimately cause venting of fluids to the atmosphere. (b) Schematic details of the two main fluid-producing processes occurring together in an aureole; kerogen cracks to methane, and hydrous minerals release H₂O during prograde metamorphic reactions. (c) The final aureole is consisting of an inner aureole defined by vitrinite reflectance $>1.5\%$ Ro where only gas is generated and an outer aureole defined by $>0.5\%$ Ro, where gas and potentially oil can be generated. The TOC content decreases and the %Ro increases towards the contact.

Table 1
List of studies dealing with contact metamorphism from sheet intrusions.

References	Modeling provided	Data provided	Intrusion thickness	Normalized aureole	Lithology of host-rock
Barker and Bone (1995)		V _b -Da	2.2 m	~5% D	High grade limestone
Barker et al. (1998)	T-F-L _C	V	0.06 – 40 m	30–150% ^a D	Clay/sediments
Bishop and Abbott (1995)	T	V-TOC-RE-GC	0.3–3.0 m	30–70% ^a D	Shale/silty shale
Brown et al. (1994)	T-R _o	V	40–60 m	150% ^a S	Shale/limestone
Bostick and Pawlewicz (1984)		V	3.6–10.4 m	75–100% ^a D	Shale/limestone
Clayton and Bostick (1986)		V-RE-GC-Da	1.3 m	~50% ^a D	Siltstone
Cooper et al. (2007)		V-TOC-Da	0.15–1.8 m	75–110% ^a S/D	Coal/black shale
Delaney (1982)	T-F-Me				
Dow (1977)		V	~180 m	200% ^a S	
Drits et al. (2007)		Mi	0.5–80 m	~75% ^b S	Mudstone
Dutrow et al. (2001)	T-F-R	TOC-Da	11 m	35–55% ^b D	Carbonate/siltstone
Finkelman et al. (1998)		V-RE-El-Mi	1.5 m	~35% ^a D	Coal/coke
Fjeldskaar et al. (2008)	T-R _o	V	118.5 m	~150% ^c S	Silt/shale/sandstone
Galushkin (1997)	T-F-L _C -L _D -R _o	V	0.9–118.5 m	55–170% ^a S/D	Black shale/silt
George (1992)		V-RE-GC-Da	3.5 m	~70% ^a D	Silt/oil shale
Golab et al. (2007)		Mi-El-Da	~0.1–3 m	~200% ^a D	Coal
Gröcke et al. (2009)		V-Da	1.2–1.5 m	~100% ^a D	Coal
Hanson and Barton (1989)	T-L _C -L _D			D	
Jaeger (1959)	T-F-L _V			100% ^c	
Kjeldstad et al. (2003)	T-F-P-R _o				
Litvinovski et al. (1990)	T-L _M -P		500 m	>>10% ^b D	Clay/pumice
Mastalerz et al. (2009)		V-Da	>1.2 m	~50% ^a D	Coal
Meyers and Simoneit (1999)		TOC-RE-Da	1.5 m	~60% ^b S	Coal
Othman et al. (2001)		V-RE-GC	0.40–15.7 m	S	Mudstone
Perregaard and Schiener (1979)		V-GC	4.5 m	~50% ^a D	Shale
Peters et al. (1983)		V-RE-GC	0.2–15 m	50–70% ^a S	Black shale
Polyansky and Reverdatto (2006)	T-L _M -F-R		280 m	10–70% ^c S	Sand/siltstone
Raymond and Murchison (1988)		V	50–118.5 m	~100–200% ^a S	Shale/silt/limestone
Rodriguez Monreal et al. (2009)	T-R _o -HC	V-RE-GC	110–600 m	50–100% ^a S	Black shale
Santos et al. (2009)	T	Mi-El	13 m	~90% ^b S	Carbonate/ black shale
Saxby and Stephenson (1987)		TOC-GC-Da	3 m	~50% ^b S	Oil shale
Simoneit et al. (1978, 1981)		V-TOC-GC-Da	0.2–15 m	40–50% ^a S	Black shale
Snyman and Barclay (1989)		V		50–1400% ^a D/S	Coal
Svensen et al. (2007)		V-TOC-RE	80 m	~30% ^a S	Black shale/shale
Sweeney and Burnham (1990)	T-R _o	V	10.4 m	~100% ^{a,c} D	Shale
Zhu et al. (2007)		V-GC-Da	50 m	~20% ^a S	Black mudstone

Modeling: T – thermal modeling; F – effect of fluids; L_C – latent heat of crystallization; L_D – latent heat of dehydration; L_M – latent heat of host-rock melting; L_V – latent heat of vaporization; R – mineral reactions; R_o – vitrinite modeling; HC – hydrocarbon modeling; P – pressure modeling; Me – mechanical failure.

Data: V – vitrinite; V_b – Bitumen reflectance; TOC – total organic carbon; RE – Rock-Eval analysis; GC – gas chromatography; Da – additional data; Mi – mineralogical data; El – elemental data.

Aureole: D – dike; S – sill.

^a Calculated from elevated vitrinite profiles.

^b Based on other measurement techniques.

^c Based on modeling results.

Isherwood, 2003; Nabelek, 2007). Mineral reactions in sedimentary host-rocks around sheet intrusions, which cools faster and have less heat available relative to plutons, are comparatively poorly documented. Still, it is shown that dehydration can initiate within 75% of the sill thickness around an 80 m thick intrusion (Drits et al., 2007), and also the heat from thinner intrusions (~6 m) can induce dehydration and contact melting of the host-rock (Holness and Watt, 2002).

2.3. Modeling of contact aureoles

Numerical modeling of aureole-processes has several approaches, including heat conduction with latent heat of crystallization, dehydration and melting of aureole rocks, and heat advection by fluids with or without pore-pressure buildup (e.g. Jaeger, 1959; Delaney, 1982; Litvinovski et al., 1990; Annen and Sparks, 2002). Some common modeling approaches are presented in Table 1. Only five of these studies include modeling of vitrinite reflectance. None of the previous models combine modeling of organic and inorganic reactions, nor estimations of gas generation. Most numerical models are restricted to calculations of the temperature profile around intrusions, which is not sufficient for estimating the amount and composition of fluids that can be generated from the intruded shales.

3. METHODS

We use a 2D finite element model for conductive heat-flow around a sill intrusion with latent heat of crystallization, latent heat of kerogen cracking and latent heat of dehydration reactions. The model accounts for kinetically controlled vitrinite maturation and kerogen cracking using Easy%Ro (Sweeney and Burnham, 1990) and mineral dehydration as predicted by phase equilibria (Connolly, 2009). We focus on conductive heat transfer with latent heat, and do not consider heat advection by fluid flow. This simplification is justified by analytical solutions that show negligible advective heat transport for a fluid expulsion of less than 10 wt.% through a low-permeable system, such as shales (Podladchikov and Wickham, 1994). In addition, we avoid making basin-scale assumptions about the fluid-flow regime in the host-rocks, such as permeability and true pressure gradients. Heat advection by fluids may influence the geometry of local contact aureoles, although the total heat available for reactions is constant.

Despite the relatively common use of Easy%Ro to estimate vitrinite reflectances, there has been little focus on the sensitivity of the model to varying initial parameters. We therefore conducted a series of simulations to study the response of vitrinite reflectance to the key parameters influencing the thermal input into aureoles: sill thickness; intrusion temperature; and host-rock temperature.

3.1. Thermal modeling

A numerical model is developed for solving the thermal evolution of a cooling sill using 2D finite element method

with a numerical resolution of 100 by 400 elements, and 1D finite difference method with a resolution of 1 by 500 elements. The 2D model domain is shown in Fig. 2. We assume instantaneous igneous emplacement and no post-emplacement flow. The physical parameters utilized in the modeling are given in Table 2. We use the 1D model to calculate aureole thicknesses by systematically varying the intrusion temperature from 900 to 1300 °C, the host-rock temperature from 10 to 110 °C, and the sill thickness from 1 to 150 m. The 1D model gives similar results to the 2D model, but is more time-efficient for the array of runs conducted. We solve the heat conduction equation with latent heat,

$$\frac{\partial T}{\partial t} = \frac{k}{\rho C_p^{eff}} \left(\frac{\partial^2 T}{\partial x^2} + \frac{\partial^2 T}{\partial z^2} \right) - \frac{L_{OM} R_{OM}}{\rho C_p} - \frac{L_D R_D}{\rho C_p}, \quad (1)$$

where T is temperature, ρ is density, k is thermal conductivity, C_p is heat capacity, t is time, x is horizontal direction, z is vertical direction, L is latent heat of devolatilization reactions, and R is rate of devolatilization reactions ($\text{kg}_{\text{fluid}}/\text{s}/\text{m}^3$) with formulas given in the following sections. An effective heat capacity, C_p^{eff} , accounts for the latent heat of fusion in the crystallizing parts of the sill,

$$C_p^{eff} = C_p \left(1 + \frac{L_C}{(T_L - T_S) C_p} \right) \quad \text{for } (T_S < T < T_L) \quad (2)$$

$$C_p^{eff} = C_p \quad \text{for } (T_S > T),$$

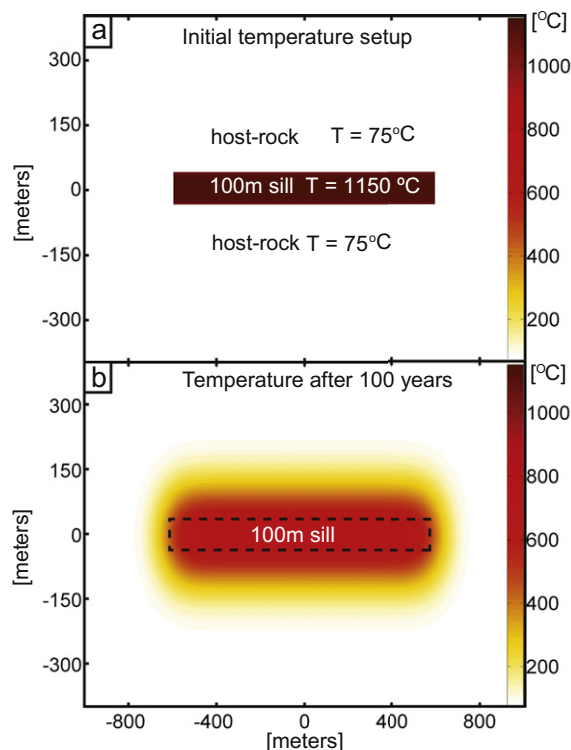


Fig. 2. Setup of the numerical model for a 100 m thick sill. (a) Initial conditions. An instantaneous emplacement of a 1150 °C sill in a host-rock of 100 °C. (b) The sill is cooling by conduction with time. Parameters used in the modeling are given in Table 2.

Table 2
Parameters used in the thermal modeling.

Symbol	Description	Value	Unit
T_m	Initial temperature of melt	1423 ^k	K
T_{hr}	Initial temperature of host-rock	348 ^k	K
T_L	Liquidus temperature	1423 ^a	K
T_S	Solidus temperature	1223 ^{a,k}	K
K_T	Thermal diffusivity ($k/\rho/C_p$)	10 ^{-6b,c}	m ² /s
ρ_m	Density melt	2600 ^b	kg/m ³
C_{pm}	Heat capacity melt	820 ^b	J/kg/K
ρ_{hr}	Density host-rock	2400 ^d	kg/m ³
C_{phr}	Heat capacity host-rock	850 ^e	J/kg/K
k	Thermal conductivity	2.1 ^{b,f}	J/K/m ³
L_C	Latent heat of crystallization	320 ^g	kJ/kg
L_D	Enthalpy of mineral dehydration	2800 ^h	kJ/kg _{H₂O}
L_{OM}	Enthalpy of organic cracking	375 ⁱ	kJ/kg _{TOC}
R	Gas constant	8.31	J/K/mol
A	Frequency factor	10 ^{13j}	1/s
E	Activation energy	142-301	kJ/mol
d	Aureole thickness		m
h	Sill thickness	1-150 ^k	m
W	Fraction of convertible organic matter pr TOC	850 ^j	g kg ⁻¹
R_{OM}	Rate of kerogen conversion into hydrocarbons		kg _{TOC} /m ³ /s
R_D	Rate of mineral dehydration reaction		kg _{H₂O} /m ³ /s
X_O	Atomic fraction of n_O relative to $n_H + n_O$		–
n_O	Number of moles of oxygen per mole fluid		–
n_H	Number of moles of hydrogen per mole fluid		–

^a Métrich and Rutherford (1998).

^b Barker et al. (1998).

^c Delaney (1982).

^d Storvoll et al. (2005).

^e Berkovich et al. (2000).

^f Reiter and Tovar (1982), for shale.

^g Turcotte and Schubert (2002).

^h Trommsdorff and Connolly (1996), average dehydration.

ⁱ Shih and Sohn (1978).

^j Sweeney and Burnham (1990).

^k This study approximations.

where L_C is latent heat of crystallization, T_L is liquidus temperature and T_S is solidus temperature of the melt. Effects of latent heat of mineral dehydration and organic cracking are accounted for by the enthalpy method.

The boundary conditions are fixed to the host-rock temperature at the top and bottom of the domain, while the boundary conditions at the sides are free. The boundaries do not influence the developing thermal field. We assume that the host-rock temperature above and below the intrusion are equal.

3.2. Organic maturation

3.2.1. Modeling of organic maturation

The individual chemical steps during kerogen cracking are complex and to a large degree unknown (e.g. Beardmore and Cull, 2001). However, it has been shown for a bulk organic system that the rate of maturation can be satisfactorily approached by the Arrhenius equation using a set of 20 parallel first order reactions,

$$k_i = A \exp(-E_i/RT) \quad (3)$$

where A is the frequency factor, R is the gas constant and E_i is the activation energy for the i th reaction (e.g. Tissot et al., 1987; Ungerer and Pelet, 1987). The parallel reactions (i) represent the breaking of different kerogen bonds. We utilize the model Easy%Ro developed by Sweeney and Burnham (1990) for consistent modeling of vitrinite reflectance and organic cracking reactions. It is based on an average set of kerogen maturation kinetics and conveniently implemented using the following approach. The Arrhenius equation is integrated over time,

$$I_{it} = \int_0^t A \exp(-E_i/RT) dt, \quad (4)$$

in order to calculate the decrease in the initial amount of convertible material (W_{i0}),

$$W_{it} = W_{i0} \exp(-I_{it}). \quad (5)$$

where W_{it} is the mass fraction of convertible material at time t . The total amount of product released at time t , Q_t , is

$$Q_t = \sum_i W_{i0} - W_{it} \quad (6)$$

The vitrinite reflectance is a widely used parameter to determine the organic maturity of the source rock (Dow, 1977; Hunt, 1996). The calculation of vitrinite reflectance is implemented following the recipe of Easy%Ro by

$$\%Ro = \exp(-1.6 + 3.7F), \quad (7)$$

where

$$F = \sum_i f_i \left(1 - \frac{W_i}{W_{i0}}\right) \quad (8)$$

and f_i is the weighting factor for the i th reaction. Values for E_i and f_i can be found in Sweeney and Burnham (1990). From this model it is apparent that the minimum value of %Ro is $\exp(-1.6) = 0.2$ when $F = 0$, and at maximum conversion ($F = 0.85$) the value of %Ro is $0.2 \times \exp(3.7 \times 0.85) = 4.7$. At maximum conversion, 15% of the initial TOC content is retained as a graphite residue in the model. This corresponds to behaviour of kerogen between Type I and II, compatible with the organic-rich shale formations in the Karoo Basin (Faure and Cole, 1999).

Fig. 3 shows the result of the numerical model compared to normalized vitrinite reflectance data from a 10.4 m thick sill using the reported thermal values $T_{hr} = 30$ °C and $T_{melt} = 1240$ °C (Bostick and Pawlewicz, 1984). The error introduced by not considering latent heat effects is approximately 20% less extensive aureole. The spreading of the data is by comparison 10–20%.

The reaction rate of hydrocarbon generation R_{OM} is coupled to the organic reaction (Eq. (6)) through $R_{OM} = \rho_{hr}(\tau_{t-i} - \tau_t)$, with $\tau_t = \tau_0 - Q_t \tau_0$, where τ_t is wt.% TOC/100 at time t , and ρ_{hr} is the density of the host-rock. We use a density of 2400 kg/m³, simulating the 2–4 km deep organic-rich shale formations in the Karoo Basin (Catuneanu et al., 2005).

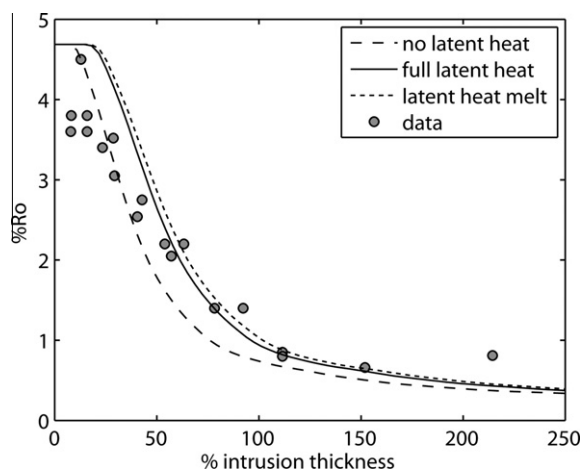


Fig. 3. Comparison of numerical calculations without (long dashed line) latent heat, with latent heat of crystallization and devolatilization (solid line) and latent heat of crystallization only (short dashed line) with data (circles) from aureoles around a 10.4 m dike (Bostick and Pawlewicz, 1984), normalized over intrusion thickness. Host-rock temperature is 30 °C and intrusion temperature is 1240 °C (Bostick and Pawlewicz, 1984), the other values used are given in Table 2.

3.2.2. Estimation of methane generation

We assume that all hydrocarbons are converted into methane (CH₄), because the kinetic conditions for transformation of organic matter at high temperatures favor gaseous products over liquid petroleum (e.g. Reverdatto and Melenevskii, 1983; Tissot and Welte, 1984; Karlsen and Skeie, 2006). We cannot exclude the generation of additional oil, although secondary cracking of oil to gas is expected to initiate around 180 °C (Schenk et al., 1997), which is reached even in the outer parts of the aureole, supporting our assumption. The CH₄ yield (kg_{CH₄}/m³_{rock}) is calculated from the relation

$$Q_{CH_4} = Q_t / 1000 \times \tau_0 \times M_f \times \rho_{hr}, \quad (9)$$

where M_f is conversion factor from C to CH₄ (1.34).

We extrapolate the calculations of gas quantities generated in one aureole to basin-scale gas generation by assuming a cumulative sill thickness of 100 m intruding into organic formations in a basin. The total amount of CH₄ generated in one vertical column with an area of 1 m² (kg m⁻²) is determined by summing up a 1D section above and below the 100 m thick sill. We only consider methane generated within %Ro ≥ 1. To get the total mass of CH₄ generated on a basin-scale, this value is multiplied with the total area intruded by sills. The total area estimated to be covered by sills in the Vøring and Møre basins is 85,000 km² (Svensen et al., 2004). However, the Vøring and Møre basins belong to the North Atlantic Volcanic Province, which is probably at least 5 times as large. The extent of sills intruding into the western Karoo Basin is ~50,000 km² based on the mapped area of vent structures (Svensen et al., 2007). For the total Karoo Basin we use an area of 390,000 km² for sills intruded into carbon-rich sediments (Svensen et al., 2007). For the Siberian Traps we use an area of 1.6 million km² based on outcropping sill intrusions (Svensen et al., 2009).

3.3. Mineral dehydration modeling

Mineral dehydration reactions are modeled to estimate the relative amounts of CH₄ and H₂O generated in aureoles for different initial wt.% TOC and sill thicknesses. The thermal solver is coupled to mineralogy by phase equilibrium modeling (Connolly, 2009). The silicate metamorphic reactions are hence assumed to occur according to local equilibrium. We use an average pelitic sediment composition after Caddick and Thompson (2008), with SiO₂ = 59.80%, Al₂O₃ = 16.57%, MgO = 2.62%, Na₂O = 1.73%, K₂O = 3.53%, CaO = 1.09%, FeO = 5.81%, TiO₂ = 0.75%, MnO = 0.10% and H₂O = 5.00%, by weight. Fig. 4a shows the calculated equilibrium mineral assemblages of the pelite, and Fig. 4b displays the bulk water content of the mineral assemblage as a function of temperature and pressure. We fix the pressure at 100 MPa, and use the transient thermal solver to extract contact aureole temperatures (along the dashed line). The total amount of H₂O generated is thus directly linked to the maximum temperature obtained in the aureole. The rate of dehydration R_D is calculated from $R_D = \rho_{hr}(\omega_{t-1} - \omega_t)$, where ω_t is wt.% H₂O/100 at time t , extracted from the relations in Fig. 4b.

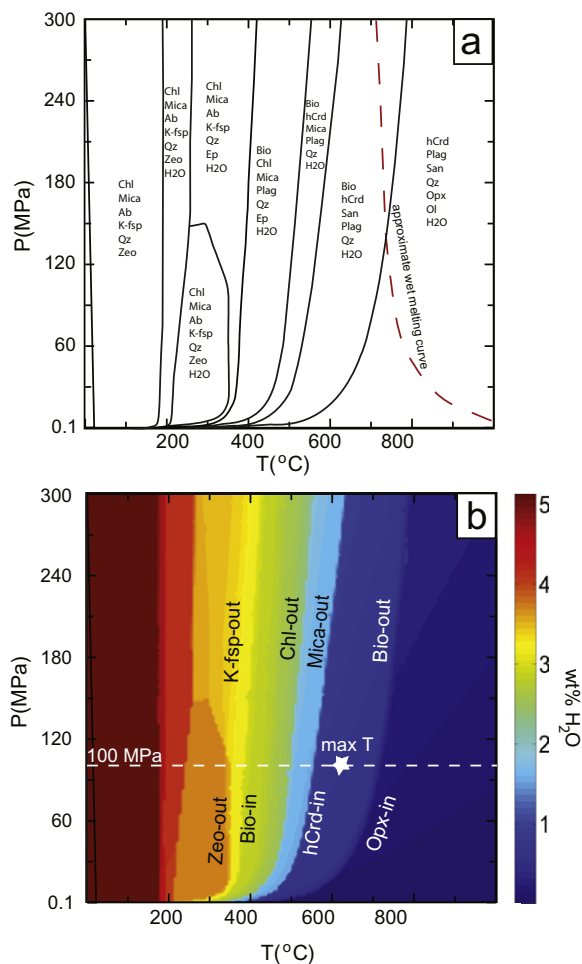


Fig. 4. (a) Stable mineral assemblages calculated from Perple_X (Connolly, 2009) for an average pelite (Caddick and Thompson, 2008). The assemblages are simplified from original calculations to consider major dehydration reactions. Wet melting may occur above ~ 750 °C as indicated by the dashed line (Nichols et al., 1994; Grant, 2004). (b) Calculated bulk maximum H_2O content as a function of pressure and temperature. The dashed line indicates where the calculations in our model are done. Maximum temperature obtained in the aureoles in this study is indicated by the star at ~ 600 °C. *Mineral abbreviations:* Ab – albite; Bio – biotite; Chl – chlorite; Ep – epidote; hCrd – hydrous cordierite; K-fsp – alkali-feldspar; Mica – white mica; Ol – olivine; OpX – orthopyroxene; Plag – plagioclase; Qz – quartz; San – sanidine; Zeo – zeolite.

3.4. Linear regression analysis

We apply linear regression analysis to our set of 1D calculations of aureole thicknesses. The modeling results are assembled in matrices which are solved for the unknown coefficients C :

$$\begin{bmatrix} \frac{d^1}{h^1} & \frac{d^n}{h^n} \end{bmatrix} = \begin{bmatrix} C_{T_{host-rock}} \\ C_{T_{intrusion}} \\ C_{\ln(h)} \\ C_1 \end{bmatrix} \begin{bmatrix} T_{host-rock}^1 & T_{intrusion}^1 & \ln(h)^1 & 1^1 \\ \vdots & \vdots & \vdots & \vdots \\ T_{host-rock}^n & T_{intrusion}^n & \ln(h)^n & 1^n \end{bmatrix}, \quad (10)$$

where d is the aureole thickness, h is the sill thickness and n is the number of calculations in this study (~ 1500), with systematic variations of sill thickness (1–150 m), intrusion temperature (900–1300 °C) and host-rock temperature (10–110 °C). The coefficients are used to construct a simple formula predicting the aureole thickness. To evaluate the accuracy of the regression model we find the coefficient of determination R^2 from

$$R^2 \equiv 1 - \frac{S_{err}}{S_{tot}}, \quad (11)$$

where S_{tot} is the total sum of squares, $S_{tot} = \sum_{i=1}^n (y_i - \bar{y}_i)^2$, where $y = (d/h)_{calculated}$ is the calculated aureole thicknesses (d) normalized over sill thickness (h) and $\bar{y} = \frac{1}{n} \sum_{i=1}^n y_i$ is the grand mean of the normalized aureole thickness; $S_{err} = \sum_{i=1}^n (y_i - z_i)^2$ is the total sum of squared errors, where $z = (d/h)_{fitted}$ for the fitted aureole thicknesses normalized over sill thickness.

3.5. Fluid composition

Fluid speciation calculations are conducted in order to derive the phase relationship between the generated H_2O and carbonic species. We calculate carbon saturated fluid phase equilibria using Perple_X using the equation of state from Connolly and Cesare (1993). Carbon-saturated fluids have only one compositional degree of freedom (X_O) which is specified by

$$X_O = \frac{n_O}{n_O + n_H}, \quad (12)$$

where n_O and n_H are number of moles of O and H per mole of fluid (Connolly, 1995). A pure CH_4 -fluid has $X_O = 0$, and a pure H_2O -fluid has $X_O = 1/3$.

4. RESULTS

4.1. Devolatilization reactions

Fig. 5 shows the results of the final reaction stages of fluid generation as a function of TOC content (1 and 5 wt.%) of the host-rocks. We define the gas zone as vitrinite reflectance larger than 1.5%Ro (gas only), and oil zone as %Ro between 0.5 and 1.5 marking the catagenetic maturation (oil + gas) (e.g. Hunt, 1996). The aureole thickness (%Ro ≥ 1) is ~ 150 m for the 100 m thick sill (Fig. 5d). The amount of CH_4 generated during heating varies greatly with the initial total organic carbon. The amount of H_2O generated in the gas zone is 25 to 107 kg/m³, decreasing to 0 kg/m³ in the oil zone (Fig. 5a). For 1 wt.% TOC, 14–27 kg/m³ CH_4 is generated in the gas zone, decreasing to ~ 10 kg/m³ hydrocarbons in the oil zone (Fig. 5b). For a shale with 5 wt.% TOC the CH_4 -generation is 70–136 kg/m³ in the gas zone, decreasing to ~ 40 kg/m³ in the oil zone (Fig. 5c). This implies that in the case of 5 wt.% TOC the amount of generated CH_4 is up to twice the amount of H_2O , although the initial wt.% of both TOC and H_2O in the rock is the same. The mass of generated gas per volume of rock is unaffected by the sill thickness. However, a larger

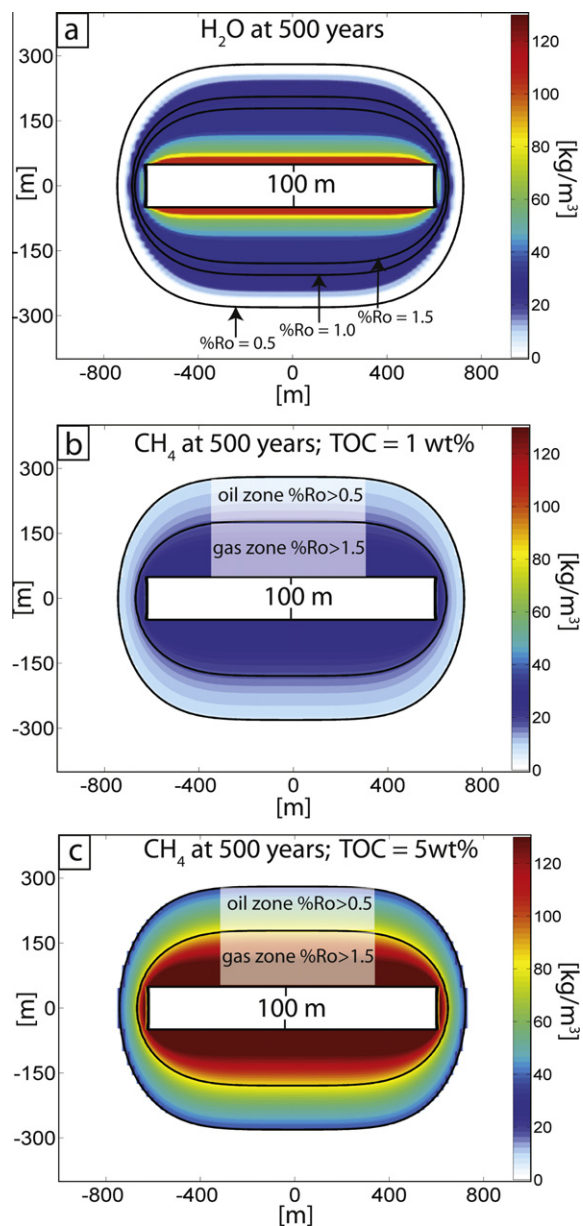


Fig. 5. Calculation of (a) H_2O , (b) CH_4 for 1 wt.% TOC and (c) 5 wt.% TOC for a 100 m thick sill emplaced at ~ 3 km depth with intrusion temperature of 1150°C and host-rock temperature of 75°C . Generated amounts are given in kg m^{-3} . The figure shows the final aureole at 500 years.

sill will affect a larger total volume of rocks and hence generate a larger total mass of CH_4 and H_2O .

4.2. Aureole thickness

To compare published data from different geological settings, we have normalized the aureole thicknesses d to the intrusion thickness h (Fig. 6a). The assembled data from Table 1 show that most aureole thicknesses fall between 30% and 200% of sill thicknesses (Fig. 6b). There is a tendency for thinner intrusions to have smaller aureoles than

thicker intrusions, although no clear distinction can be made. The distribution of observed aureole thicknesses is within the range of the systematically calculated distribution of aureole thicknesses shown in Fig. 6c.

To get a rough indication on the relative importance on the three parameters that are varied in the modeling, we apply linear regression analysis (Eq. (10)) to the series of runs conducted. This results in the following fitting formula

$$\frac{d}{h} \approx 0.0102 \cdot T_{\text{host-rock}} + 0.0029 \cdot T_{\text{intrusion}} + 0.1936 \cdot \ln(h) - 6.8611, \quad (13)$$

where d is the aureole thickness and h is the sill thickness. Fig. 7a shows a plot of the values obtained from this formula against calculated values. Most of the calculated aureole thicknesses (98.6%) are reproduced by the fitting formula to within a factor 2 (Fig. 7b). The fit is most accurate for sills of 5–20 m, but is less accurate for higher sill thicknesses. The negative fit in Fig. 7a comes from a combination of the lowest values in $T_{\text{host-rock}}$, $T_{\text{intrusion}}$ and h , giving a total value less than 6.8611. From Eq. (11), the coefficient of determination $R^2 = 0.89$, which indicates that we capture about 90% of the response of d/h in the calculations by Eq. (13). Note that this linear relationship originates from vitrinite calculations using an equation with a total of three exponents (Eq. (7)), which makes a perfect linear fit unexpected. From the formula we deduce that changing the host-rock temperature by 50°C has a larger influence on the aureole thickness than changing the intrusion temperature by 50°C . Changing the sill thickness by 50 m will have an intermediate influence. Hence, host-rock temperature is the most sensitive parameter, while sill thickness will be most important for the non-normalized aureole thickness. This suggests that the depth of sill emplacement and the geothermal gradient in the basin are important factors in determining the volume of heated sediments, and hence the total mass of generated gas.

4.3. Fluid composition

The results of fluid speciation calculations are plotted in Fig. 8a, contoured for pressure ranging from 100 to 500 MPa. The compositions of the fluids generated are calculated from average fluid composition within the gas zone (Fig. 5). We use two cases with initially 1 and 5 wt.% TOC, both with 5 wt.% H_2O . The average amount of CH_4 is 20 kg/m^3 (1259 mol/m^3) for 1 wt.% TOC and 120 kg/m^3 (7500 mol/m^3) for 5 wt.% TOC, both with 90 kg/m^3 (5000 mol/m^3) H_2O . The number of moles of O and H per mole of fluid is thus for the first case $n_{\text{O}} = 0.40$ and $n_{\text{H}} = 1.20$, and for the second case $n_{\text{O}} = 0.29$ and $n_{\text{H}} = 2.29$. Solving Eq. (12) for these two cases yields average fluid compositions in the whole aureole of $X_{\text{O}}^{1\text{wt}\%} = 0.25$ and $X_{\text{O}}^{5\text{wt}\%} = 0.11$, indicated by stars in Fig. 8a.

Fig. 8b shows the calculated densities for the expected fluid compositions for aureole temperatures and 100 MPa. The density-change of the devolatilization reactions from solid to fluid will influence the efficiency of the fluid transport from the aureole to the atmosphere. The density for the CH_4 -dominated fluid ranges from 140 to 350 kg/m^3 ,

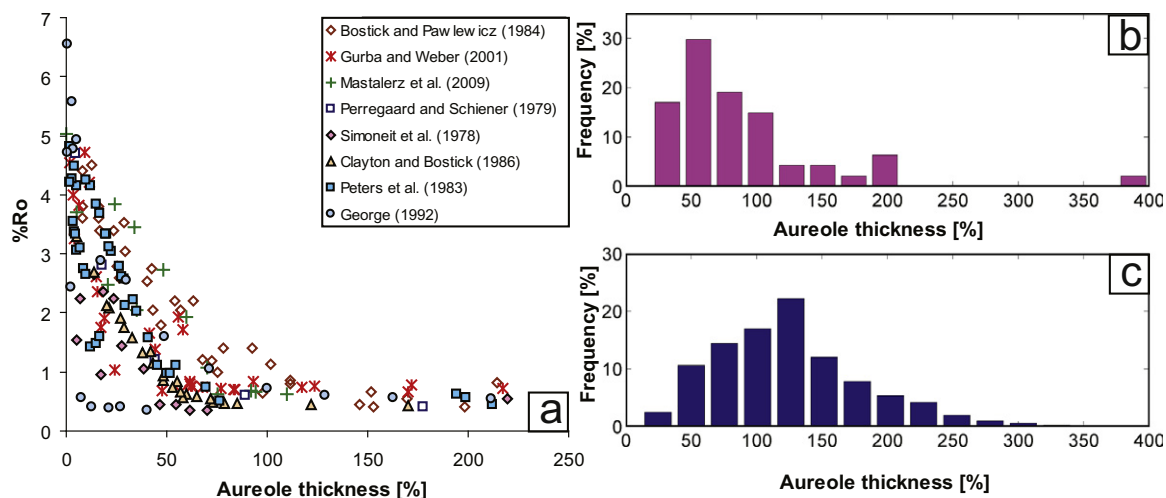


Fig. 6. (a) Vitrinite profiles from several sill intrusions of various thicknesses plotted as a function of normalized aureole thicknesses. There is a large diversity in the profiles, although all profiles show an increase from $\sim 0.5\%$ to 1% Ro up to $\sim 5\%$ Ro at the contact. (b) Relative aureole thicknesses based on elevated vitrinite reflectance varying from $\sim 30\%$ to 400% sill thickness (Table 1). (c) Calculated relative aureole thicknesses based on $\%Ro > 1$, for varying sill thickness and temperature of intrusion and host-rock.

and the H_2O -dominated fluid ranges from 800 to 900 kg/m³. Because pure H_2O do not boil at these pressures, the change in density from solid to fluid upon dehydration is about one magnitude lower than the density change going from solid to CH_4 .

4.4. Basin-scale gas generation

Fig. 9 shows the total CH_4 generated in the aureoles around basin-scale sill-complexes emplaced in shale from 0.5 to 10 wt.% TOC. This analysis is relevant to understand gas generation in sedimentary basins affected by LIPs. For a background shale with 1–6 wt.% TOC, the estimated CH_4 generation potential for the Vøring and Møre basins is ~ 600 – 3500 Gt (Fig. 9). The total production potential for the Karoo Basin ranges from ~ 2700 to $\sim 16,200$ Gt (for 1–6 wt.% TOC). The source of carbon in the Karoo Basin is mainly the organic rich Ecca Group, including the black shale of the Whitehill Formation of 2–8 wt.% TOC and the Prince Albert Formation of 0.5–4 wt.% TOC (Svensen et al., 2007). With an average TOC content of 2–4 wt.%, a conservative estimate of the methane produced in the Karoo Basin is ~ 5400 – $10,700$ Gt.

The Siberian Traps were responsible for massive contact metamorphism and enhanced maturation in the Tunguska Basin, Russia (e.g. Kontorovich et al., 1997). We estimate that at least $\sim 12,000$ – $66,000$ Gt of CH_4 (for 1–6 wt.% TOC) could have been generated through contact metamorphism of organic material in the Tunguska Basin, using the same upscaling approach as for the other basins.

5. DISCUSSION

5.1. Modeling of contact metamorphism in shales

5.1.1. Heat flow model

Latent heat of pore-water vaporization may be a heat sink in shallow intrusions, but because we consider deeply

buried shales (~ 3 km) with low porosity, we do not incorporate this effect, as vaporization of pure H_2O is confined to the upper ~ 1 km of a sedimentary basin (Kokelaar, 1982; Wagner and Pruss, 2002).

We have assumed no additional heat transport by fluid flow (i.e. the Peclet number is zero) as a first-order approximation for our basin-scale estimations. Although not shown here, there is a tendency for larger aureoles to occur above sills than below (e.g. Simoneit et al., 1978; Peters et al., 1983; Gurba and Weber, 2001). The asymmetry may result from vertical heat transport by fluids (e.g. Kjeldstad et al., 2003). However, conduction is expected to be the main heat-transfer process in low-permeable shale sequences due to limited pore-water convection (e.g. Connolly and Thompson, 1989; Podladchikov and Wickham, 1994). The zone of vertical fracturing is only making up 10–20 cm at the contact zone around a 10 m thick sill in South Africa (Aarnes et al., in review-b). Moreover, the application of this model to %Ro and TOC data from the Karoo Basin gives a good agreement between modeling and data without considering heat advection by the fluids (Aarnes et al., in review-b), supporting our assumption.

5.1.2. Gas generation

Using default kinetic parameters from Easy%Ro that were determined from a wide range of source rocks is ideal for our generalised numerical approach to basin-scale aureole processes. The total generation potential W used in Easy%Ro adds up to 850 g_{H₂C}/kg_{rock}, similar to Type I kerogen, while the broad distribution of activation energies (142–301 kJ/mol) resembles the behaviour of Type III kerogen (Ungerer and Pelet, 1987). Thus, the overall behaviour of kerogen transformation in shale source-rocks in our model is maintained. The application of default kinetics parameters implies that our model cannot explain all case studies, due to a vast array of kinetic responses in different rock types (e.g. Snowdon, 1979; Peters et al., 2006).

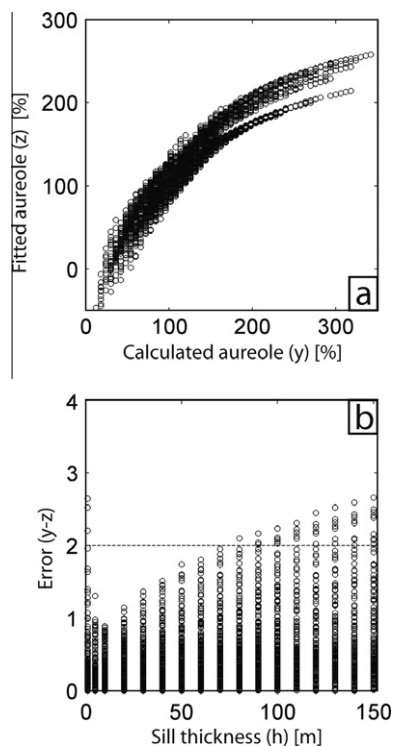


Fig. 7. (a) Calculated aureole thicknesses from numerical simulations (y) plotted versus fitted aureole thicknesses (z) (Eq. (13)). About 90% of the data can be reproduced by a plane involving intrusion and host-rock temperature, as well as the natural logarithm of the sill thickness. The negative fit in z arises from extreme conditions, when the values of host-rock, intrusion and sill thickness is at its lowest (e.g. 10 °C, 900 °C and 1 m, respectively) in Eq. (13). This is a quite unlikely scenario, and not too much attention should be paid to the negative numbers. (b) Differences between calculated and fitted aureole thicknesses (error) are approximately within a factor 2 (dashed line), i.e. the fitting formula (Eq. (13)) gives a good indication of the calculated aureole thickness arising from heat conduction within a factor 2 error. The fitting formula is most accurate for sills around 5–20 m, with progressive less accuracy with increasing (and decreasing) sill thickness.

The type of kerogen in heated sediments dictates how much gas can be generated. Humic coals are mainly composed of Type III kerogen from which 10–25% of the carbon mass can be converted into gas (e.g. Hunt, 1996). In contrast, Type I and II kerogen commonly found in organic-rich shales have the potential of converting up to 95% of the TOC to hydrocarbons (e.g. Ungerer and Pelet, 1987). Because we use a conversion factor of 85% by weight, our approach will lead to an overestimation of gas generated from coal source rocks. Moreover, a considerable proportion of the carbon gases generated in coals can be retained with a high trapping efficiency within the structure of coals (Behar and Vandenbroucke, 1988; Saghafi et al., 2007, 2008). Precipitation of carbonates derived from coal decomposition and CO_2 can also cause further retention of the carbon gases in coal (Finkelman et al., 1998; Golab and Carr, 2004). Coals are therefore less important for generating and releasing large volumes of CH_4 gases compared

to black shales. Nevertheless, there are several case studies that demonstrate gas generation in coal that has experienced contact metamorphism (e.g. Snyman and Barclay, 1989; Cooper et al., 2007). Although not considered here, coal-derived carbon gases may add to the total basin-scale gas generation (McElwain et al., 2005).

5.1.3. Isotope fractionation during gas generation

The isotopic composition of the generated gases is important when comparing the amount of released gases to the proxy records. A recent study by Gröcke et al. (2009) suggests that the generation potential of ^{13}C -depleted carbon gases from coals is low because of the observed lack of ^{13}C enrichment in residual kerogen towards intrusion contacts. The negative fractionation of CH_4 relative to kerogen is commonly believed to cause a corresponding enrichment in $\delta^{13}\text{C}$ in the residual kerogen. However, experiments show no simple relationship between residual kerogen composition (change $\pm 2.5\text{‰}$) and the gas generated (CH_4 with $\delta^{13}\text{C}$ of -27.8 to -38.0‰) (Andresen et al., 1995; Lorant et al., 1998). For example, CO_2 has a positive fractionation of about 1–3‰ for coals, and 3–5‰ for shales (Andresen et al., 1995). Hence, we expect that a large generation of CO_2 can contribute to the small lowering of $\delta^{13}\text{C}$ values in the residual carbon. Indeed, some coals have a correlation between higher maturity and more negative $\delta^{13}\text{C}$ of kerogen (Andresen et al., 1995; Cooper et al., 2007; Schimmelmann et al., 2009). More commonly, studies report no significant shift in $\delta^{13}\text{C}$ of the residual kerogen with increasing coal maturity (e.g. Faure, 1986; Ripley and Taib, 1989; Whiticar, 1996), even when methane with $\delta^{13}\text{C}$ values from -50 to -25‰ is released (Andresen et al., 1995; Cramer et al., 1998). Due to the lack of response in residual kerogen in addition to several factors influencing the $\delta^{13}\text{C}$ values, it is speculative to use residual kerogen $\delta^{13}\text{C}$ values as proxy for the generation of isotopically light carbon gases (cf. Gröcke et al., 2009).

5.1.4. Dehydration of minerals

The advantage of the thermodynamic equilibrium approach compared to kinetic modeling is that kinetics of mineral reactions are often poorly constrained (e.g. Nabelek, 2007). An overstepping temperature needed for dehydration reactions are estimated from kinetic modeling to be rarely more than a few degrees, with a maximum of 40 °C (Walther and Wood, 1984), and would only lead to a minor shift of the equilibrium reaction conditions (Fig. 4).

The rate of dehydration reactions depends primarily on the rate of heat input (e.g. Walther and Orville, 1982). Dehydration reactions at contact aureole temperatures (~ 500 °C) are estimated to go to completion within ~ 200 years (Walther and Wood, 1984). This is well within the cooling time of 100 m sills (~ 500 – 1000 years). For thinner, 10 m sills the time of elevated temperature in the aureole may be too short for the minerals to reach equilibrium (~ 10 – 50 years). Heating experiments on oil shales show a water loss of ~ 40 kg/m^3 , using the reported shale density of 2200 kg/m^3 (Gregg et al., 1981). This is in agreement with the lower range predicted by our numerical model.

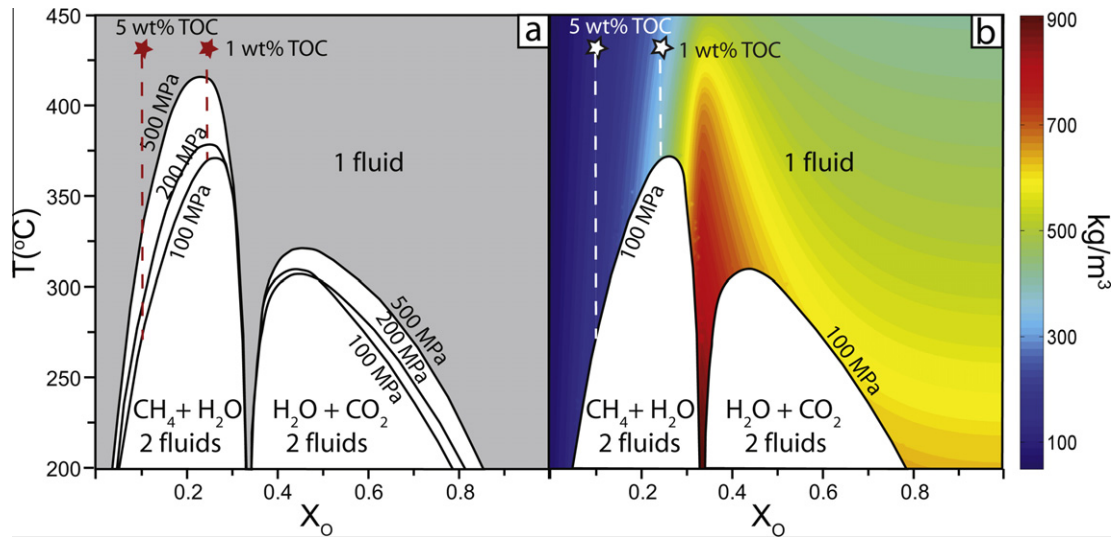


Fig. 8. (a) Fluid speciation phase diagram calculated from *Perple_X* for a carbon saturated system, using the equation of state from Connolly and Cesare (1993) contoured for pressures ranging from 100 to 500 MPa. For 1 wt.% TOC there will be miscibility between water and methane at ~ 375 °C, while fluids in rocks of 5 wt.% TOC are miscible at ~ 275 °C, for thermodynamic pressures of 100–200 MPa. (b) Calculated densities of the fluid(s) at 100 MPa. At this pressure the CH_4 -dominated phase will have a relatively low density of ~ 200 kg/m^3 , while the H_2O -dominated phase will have a relatively much higher density of ~ 900 kg/m^3 .

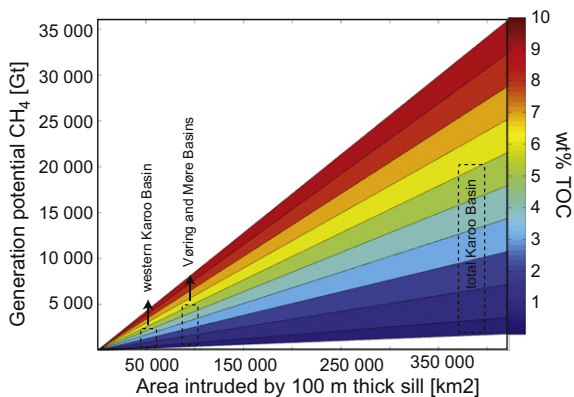


Fig. 9. Calculated total methane potential in gigatons, (Gt) as a function of area covered by a cumulative intrusion thickness of 100 m continuous sill. The generation potentials are for the western Karoo Basin ($50,000$ km^2) ~ 400 – 2100 Gt CH_4 , the Vøring and Møre basins ($85,000$ km^2) ~ 600 – 3500 Gt CH_4 and the total Karoo Basin ($390,000$ km^2) ~ 2700 – $16,200$ Gt CH_4 , for values of reacted shales from 1 to 6 wt.% TOC.

5.2. Aureole thickness

We show that the existing “rule of thumb” predicting aureole thicknesses of about 100% of the sill thickness can be improved to involve the temperatures of host-rock and intrusion, in addition to the sill thickness (Eq. (13)). The non-linear response of aureole thickness to sill thickness also implies that no universal 1:1 relationship can be expected, as thicker sills will have relatively thicker normalized aureoles. This is due to a longer total time for the heat pulse to pass through the rocks in the case of thicker sills. The derived relationship is consistent with a large diversity

in the data (Fig. 6a and b), and is further supported by a vitrinite data showing a relation between the logarithm of intrusion thickness and the aureole thickness (Raymond and Murchison, 1988). The calculated relationship is less accurate for a combination of extreme values in temperatures and sill thickness, such as a 1 m sill with T_m of 900 °C and T_{hr} of 10 °C.

An important implication of the relationship in Eq. (13) is that we expect larger aureoles to occur when sills intrude into host-rocks of relatively high background temperatures, as long as the temperature is within the field of normal organic maturation. Thus, thicker aureoles will develop in basins with high geothermal gradients or around deeply emplaced sills. This is illustrated in Fig. 10a using Eq. (13) showing aureole thicknesses as a function of different geothermal gradients. The figure is calculated using a sill thickness of 50 m and a constant intrusion temperature of 1150 °C. Fig. 10b illustrates how sill thicknesses influence the aureole thicknesses with depth. The geothermal gradient is fixed at 20 °C/km, with a constant intrusion temperature of 1150 °C. In a volcanic basin, multiple sill intrusions can cause larger aureoles due to elevated background temperatures (Hanson and Barton, 1989; Deyoreo et al., 1991; Aarnes et al., in review-b).

5.3. Composition and fate of fluids

Contact aureoles in shales will be dominated by CH_4 – H_2O fluids rather than H_2O – CO_2 fluids, because of low oxygen fugacity resulting from a lack of oxygen sources (Connolly and Cesare, 1993). This fits well with our assumption of kerogen converting mainly into CH_4 , rather than CO_2 . At 100 MPa the solubility of CH_4 in H_2O is 0.4–10 wt.% for the temperature range 100–350 °C (Bonham, 1978). This implies that for an aureole with 5 wt.% TOC,

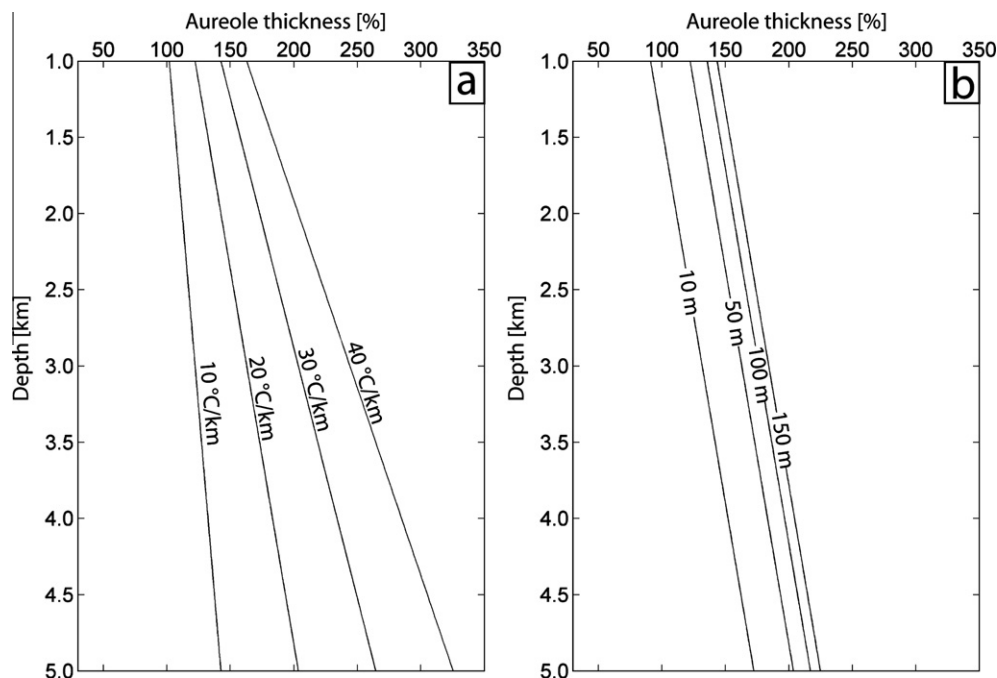


Fig. 10. Calculated aureole thicknesses as a function of geothermal gradient (a) and sill thickness (b) using Eq. (13). In (a) the sill thickness is set to 50 m, whereas the geothermal gradient is fixed at 20 °C/km in (b). A sill temperature of 1150 °C is applied in both cases.

the maximum of $\sim 20 \text{ kg/m}^3 \text{ CH}_4$ can be retained in the denser, less mobile H_2O -dominated phase (10% of $120 \text{ kg/m}^3 \text{ CH}_4 + 90 \text{ kg/m}^3 \text{ H}_2\text{O}$).

Substantial addition of CO_2 from decarbonation or sources rich in Type III-kerogen can lead to a shift towards H_2O - CO_2 fluids (e.g. Gregg et al., 1981; Finkelman et al., 1998). Also, H_2O can react with residual graphite to produce CH_4 - CO_2 fluids, with composition depending on the redox conditions (e.g. Pattison, 2006; Boiron et al., 2007). Fluid inclusion studies of metapelitic aureoles is compatible with such a scenario, with an initial CH_4 - H_2O fluid later transforming to a H_2O - CO_2 fluid as H_2O reacts with residual graphite (Huff and Nabelek, 2007).

The fates of the generated fluids will depend on their relative densities, capillary pressures and overpressure buildup, among others (e.g. England et al., 1987; Jamtveit and Yardley, 1997). A fluid-pressure buildup in the aureole will promote fluid flow out of the aureole either by seepage through microfractures, or by explosive venting. The low density of the CH_4 -fluid generated in the aureole is favorable for generating a significant fluid overpressures (Aarnes et al., in review-a). Fluid-expansion resulting from kerogen cracking to gas is a well established source of overpressure in shales (e.g. Osborne and Swarbrick, 1997; Tingay et al., 2009). The extra porosity generated from devolatilization can cause viscous compaction and initiation of porosity-waves, which provides an effective transport mechanism to the atmosphere (e.g. Connolly, 1997; Connolly and Podladchikov, 1998; Appold and Nunn, 2002).

If a large volume of rock undergoes contact-metamorphic devolatilization reactions more rapidly than the fluids can escape, the building up of overpressure may eventually be released through extensive brecciation of the rock (Aar-

nes, 2010). Pipe-like flow structures originating from contact aureoles are evidence of such overpressures (e.g. Skinner and Marsh, 2004; Oliver et al., 2006; Svensen et al., 2006). An overpressurized aureole can arise from boiling and expansion of pore-fluids down to depths of $\sim 1 \text{ km}$ (Delaney, 1982; Kokelaar, 1982; Manning and Bird, 1991; Jamtveit et al., 2004). Deeper pipe-structures rooted down to 2–4 km are thus more likely to form due to generation of substantial masses of CH_4 and H_2O in aureoles (Svensen et al., 2006, 2007). Vents are observed to commonly originate at sill tips (Planke et al., 2005). Thus, vents can drain aureole fluids from both upper and lower aureoles through lateral flow (cf. England et al., 1987). A typical pipe source region can be on the order of 5 km^3 , effectively draining the aureole systems of the generated fluids (Svensen et al., 2009).

5.4. Climate implication of basin-scale gas generation

Previous studies have suggested that the formation and release of greenhouse gases during metamorphism, such as CO_2 from decarbonation, can have an impact on the global climate (Kerrick and Caldeira, 1993, 1998). Throughout geologic history, formation of Large Igneous Provinces in sedimentary basins has coincided with episodes of global warming and mass extinctions (e.g. Wignall, 2001; Courtillot and Renne, 2003). These provinces include the Emeishan volcanic province (end-Guadalupian event, $\sim 260 \text{ Ma}$) (e.g. Zhou et al., 2002; Ganino and Arndt, 2009), the Siberian Traps (end-Permian event, $\sim 252 \text{ Ma}$) (e.g. Visscher et al., 2004; Retallack and Jahren, 2008; Svensen et al., 2009), the Central Atlantic magmatic province (Triassic-Jurassic event, $\sim 200 \text{ Ma}$) (e.g. McElwain et al.,

1999; Courtillot and Renne, 2003), the Karoo igneous province (Toarcian event, ca. 182.6 Ma) (e.g. Jenkyns and Clayton, 1997; Svensen et al., 2007, 2008) and the North Atlantic igneous province (PETM, ca. 55.5 Ma) (e.g. Svensen et al., 2004; Storey et al., 2007). All these events also coincide with global carbon cycle perturbations in the form of a negative shift in the global $\delta^{13}\text{C}$ isotopic record, which can be explained by a massive release of $\delta^{13}\text{C}$ -depleted gases, such as thermogenic methane, to the atmosphere.

Commonly, thick sills (>100 m) covering several square kilometers are found in deep levels of many sedimentary basins (e.g. Mjelde et al., 1998; Chevallier and Woodford, 1999; Polteau et al., 2008). This implies a relatively high host-rock temperature (~ 75 – 100 °C) and potentially elevated background maturation at the time of the LIP formations. In our model, these conditions support the formation of thick aureoles (Eq. (13)). If the intruded shale is mature, the original source-rock potential is decreased and the kinetic behaviour of the kerogen will be dictated by higher activation energies as the most labile bonds break off in the initial maturation. This is not accounted for in our modeling, but can be approached by using a TOC content that corresponds to the level of background maturation in the basin. We therefore assume that the host-rocks have a maximum average of 6 wt.% TOC on the basin-scale, although individual shale-formations can have initial TOC contents of at least 10 wt.%.

The calculated amounts of CH_4 generated in the Vøring and Møre basins in Fig. 9 are similar to the ~ 1340 Gt CH_4 that was estimated for a 200 m thick aureole (i.e. ~ 100 m thick sill) at 2 wt.% TOC by Svensen et al. (2004). This is a conservative value as the cumulative sill thickness in the volcanic basins can reach at least 300 m. Sill emplacement in the Vøring and Møre basins has been linked to the PETM event, with sills dated to 55.6 ± 0.3 Ma and 56.3 ± 0.4 Ma (Svensen et al., 2010).

Comparing our estimate of 3500 Gt CH_4 generated in the Vøring and Møre basins to calculations of Pagani et al. (2006) give a -2.5‰ negative shift of $\delta^{13}\text{C}$ using an isotopic composition of the released methane of -35‰ . This is compatible with the recorded $\delta^{13}\text{C}$ -drop of -2 to -3‰ (Dickens et al., 1995; Higgins and Schrag, 2006). For our least conservative estimate using 300 m of cumulative sill thickness in the Vøring and Møre basins, ~ 4000 Gt C (5250 Gt CH_4) can be generated to match the higher estimates (4000 Gt C with $\delta^{13}\text{C}$ of -35‰) required by the study of Panchuk et al. (2008).

The values calculated for the western Karoo Basin (Fig. 9) coincide well with the values 394–675 Gt CH_4 estimated by Svensen et al. (2007) based on actual aureole measurements. Similarly, the calculated methane generation potential for the total Karoo Basin (2700–16,200 Gt) corresponds well with the estimates ranging from 2505 to 10,037 Gt CH_4 for a TOC-interval of 2–5 wt.% and cumulative sill thickness of 100–200 m (Svensen et al., 2007). Rapid release of these gases would result in a $\delta^{13}\text{C}$ -drop of -3‰ to -5‰ (Pagani et al., 2006), which is similar to the proxy record for the Toarcian event (Beerling and Brentnall, 2007; Cohen et al., 2007).

Our study thus suggests rapid production (i.e. 10–1000 years) of thermogenic methane, with total masses large enough to explain the corresponding proxy records if released. The generated aureole gases can efficiently reach the atmosphere through the many (>1000) observed vent complexes (Svensen et al., 2007). The rate-limiting process will therefore mainly be the duration of sill-emplacment in organic-rich formations, as both cracking and subsequent venting are relatively rapid processes. A massive release of methane from contact aureoles can trigger positive feedback mechanisms, such as release of methane from gas hydrates (e.g. Dickens et al., 1995; Hesselbo et al., 2000) and decreased overall storage capacity of carbon in the Earth system (e.g. Cox et al., 2000; Friedlingstein et al., 2006). The advantages of the thermogenic gas release over the methane hydrate mechanism are: (1) no requirement of any pre-warming episode; (2) the existence of geological evidences that hydrocarbons were generated, and released, from basin-wide occurring contact aureoles; (3) the generation potential of methane is in the same magnitude required to explain the proxy data, which may not be the case for the methane hydrate source (Higgins and Schrag, 2006; Panchuk et al., 2008); (4) a coherent explanation of the coincidental timing of LIP formation and global carbon-cycle perturbations.

6. CONCLUSIONS

We have developed a numerical model that predicts aureole thicknesses, gas generation and mineral dehydration for a wide range of intrusion thicknesses, intrusion temperatures and host-rock temperatures. By extrapolating our model to basin-scales, we are able to estimate information about aureoles that are directly observable. Our key conclusions are:

- Aureole thicknesses can vary from $\sim 30\%$ to 200% of the sill thickness, depending on host-rock temperature, sill thickness and intrusion temperature.
- Contact metamorphism of shale will produce mainly CH_4 – H_2O fluids. CH_4 will dominate for TOC contents of >5 wt.%, while H_2O will dominate for TOC contents of <1 wt.%.
- Conversion of organic material to hydrocarbons in contact aureoles is a rapid process (10–1000 years) depending on intrusion thickness. The rate-limiting factor for hydrocarbon generation is the duration of sill emplacement.
- We estimate that the generation potential of CH_4 is ~ 600 – 3500 Gt from the Vøring and Møre basins, ~ 2700 – $16,200$ Gt from the Karoo Basin and $\sim 12,000$ – $66,000$ Gt from the Tunguska Basin. The key parameters are sill volume and TOC content of the intruded shale formations.
- Thermogenic gas generation related to LIP formations in sedimentary basins, with subsequent release of these gases to the atmosphere provides a causal connection for triggering global carbon cycle and environmental

perturbations in times of LIP formation, like the end-Permian (~252 Ma), the Toarcian (~183 Ma) and the Paleocene-Eocene (~55.5 Ma).

ACKNOWLEDGMENTS

This study is supported by Grant 169457/S30 from the Norwegian Research Council. We thank B. Jamtveit and S. Planke for important ideas, discussion and for initiation of this project. We thank D.A. Karlsen and M. Dabrowski for important input and discussions. M. Aerts and G. Gisler are thanked for improving earlier versions of this manuscript. The associate editor Thomas Chacko, Kurt Bucher and two anonymous referees are thanked for detailed comments that helped improving the manuscript.

REFERENCES

- Aarnes I. (2010) Sill emplacement and contact metamorphism in sedimentary basins. Local processes with global implications. Ph. D. thesis, University of Oslo. 181 pp.
- Aarnes I., Podladchikov Y. Y. and Svensen H. (in review-a) Fluid overpressure and rate of devolatilization during metamorphism. *J. Geophys. Res. Solid Earth*.
- Aarnes I., Svensen H., Polteau S., and Planke S. (in review-b) Contact metamorphic devolatilization of shales in the Karoo Basin, South Africa, and the effects of multiple sill intrusions. *Chem. Geol.*
- Andresen B., Thronsdon T., Råheim A. and Bolstad J. (1995) A comparison of pyrolysis products with models for natural gas generation. *Chem. Geol.* **126**(3–4), 261–280.
- Annen C. and Sparks R. S. J. (2002) Effects of repetitive emplacement of basaltic intrusions on thermal evolution and melt generation in the crust. *Earth Planet. Sci. Lett.* **203**(3–4), 937–955.
- Appold M. S. and Nunn J. A. (2002) Numerical models of petroleum migration via buoyancy-driven porosity waves in viscously deformable sediments. *Geofluids* **2**(3), 233–247.
- Barker C. E. and Bone Y. (1995) The minimal response to contact metamorphism by the Devonian Buchan Caves Limestone, Buchan Rift, Victoria, Australia. *Org. Geochem.* **22**(1), 151–164.
- Barker C. E., Bone Y. and Lewan M. D. (1998) Fluid inclusion and vitrinite-reflectance geothermometry compared to heat-flow models of maximum paleotemperature next to dikes, western onshore Gippsland Basin, Australia. *Int. J. Coal Geol.* **37**(1–2), 73–111.
- Beardmore G. R. and Cull J. P. (2001) *Crustal Heat Flow*. Cambridge University Press.
- Berling D. J. and Brentnall S. J. (2007) Numerical evaluation of mechanisms driving Early Jurassic changes in global carbon cycling. *Geology* **35**(3), 247–250.
- Behar F. and Vandembroucke M. (1988) Characterization and quantification of saturates trapped inside kerogen – implications for pyrolysate composition. *Org. Geochem.* **13**(4–6), 927–938.
- Berkovich A. J., Levy J. H., Schmidt S. J. and Young B. R. (2000) Heat capacities and enthalpies for some Australian oil shales from non-isothermal modulated DSC. *Thermochim. Acta* **357–358**, 41–45.
- Bishop A. N. and Abbott G. D. (1995) Vitrinite reflectance and molecular geochemistry of Jurassic sediments – the influence of heating by tertiary dykes (Northwest Scotland). *Org. Geochem.* **22**(1), 165–177.
- Boiron M. C., Cathelineau M., Ruggieri G., Jeanningros A., Gianelli G. and Banks D. A. (2007) Active contact metamorphism and CO₂–CH₄ fluid production in the Larderello geothermal field (Italy) at depths between 2.3 and 4 km. *Chem. Geol.* **237**(3–4), 303–328.
- Bonham L. C. (1978) Solubility of methane in water at elevated temperatures and pressures. *AAPG Bull.* **62**(12), 2478–2481.
- Bostick N. H. and Pawlewicz M. J. (1984) Paleotemperatures based on vitrinite reflectance of shales and limestones in igneous dike aureoles in the Upper Cretaceous Pierre Shale, Walsenburg, Colorado. In *Hydrocarbon Source Rocks of the Greater Rocky Mountain Region* (eds. J. G. Woodward, F. F. Meissner and C. J. Clayton). Rocky Mountain Association of Geologists. pp. 387–392.
- Brown R., Gallagher K. and Duane M. (1994) A quantitative assessment of the effects of magmatism on the thermal history of the Karoo sedimentary sequence. *J. Afr. Earth Sci.* **18**(3), 227–243.
- Caddick M. J. and Thompson A. B. (2008) Quantifying the tectono-metamorphic evolution of pelitic rocks from a wide range of tectonic settings: mineral compositions in equilibrium. *Contrib. Mineral. Petrol.* **156**(2), 177–195.
- Catuneanu O., Wopfner H., Eriksson P. G., Cairncross B., Rubidge B. S., Smith R. M. H. and Hancox P. J. (2005) The Karoo Basins of south-central Africa. *J. Afr. Earth Sci.* **43**(1–3), 211–253.
- Chevallier L. and Woodford A. (1999) Morpho-tectonics and mechanism of emplacement of the dolerite rings and sills of the Western Karoo, South Africa. *S. Afr. J. Geol.* **102**(1), 43–54.
- Clayton J. L. and Bostick N. H. (1986) Temperature effects on kerogen and on molecular and isotopic composition of organic matter in Pierre Shale near an igneous dike. *Org. Geochem.* **10**(1–3), 135–143.
- Cohen A. S., Coe A. L. and Kemp D. B. (2007) The Late Palaeocene Early Eocene and Toarcian (Early Jurassic) carbon isotope excursions: a comparison of their time scales, associated environmental changes, causes and consequences. *J. Geol. Soc. London* **164**(6), 1093–1108.
- Connolly J. A. D. (1995) Phase-diagram methods for graphitic rocks and application to the system C–O–H–FeO–TiO₂–SiO₂. *Contrib. Mineral. Petrol.* **119**(1), 94–116.
- Connolly J. A. D. (1997) Devolatilization-generated fluid pressure and deformation-propagated fluid flow during prograde regional metamorphism. *J. Geophys. Res. Solid Earth* **102**(B8), 18149–18173.
- Connolly J. A. D. (2009) The geodynamic equation of state: what and how. *Geochem. Geophys. Geosyst.* **10**.
- Connolly J. A. D. and Cesare B. (1993) C–O–H–S fluid composition and oxygen fugacity in graphitic metapelites. *J. Metamorph. Geol.* **11**(3), 379–388.
- Connolly J. A. D. and Podladchikov Y. Y. (1998) Compaction-driven fluid flow in viscoelastic rock. *Geodin. Acta* **11**(2–3), 55–84.
- Connolly J. A. D. and Thompson A. B. (1989) Fluid and enthalpy production during regional metamorphism. *Contrib. Mineral. Petrol.* **102**(3), 347–366.
- Cooper J. R., Crelling J. C., Rimmer S. M. and Whittington A. G. (2007) Coal metamorphism by igneous intrusion in the Raton Basin, CO and NM: implications for generation of volatiles. *Int. J. Coal Geol.* **71**(1), 15–27.
- Courtillot V. E. and Renne P. R. (2003) On the ages of flood basalt events. *CR Geosci.* **335**(1), 113–140.
- Cox P. M., Betts R. A., Jones C. D., Spall S. A. and Totterdell I. J. (2000) Acceleration of global warming due to carbon-cycle feedbacks in a coupled climate model. *Nature* **408**(6809), 184–187.

- Cramer B., Krooss B. M. and Littke R. (1998) Modelling isotope fractionation during primary cracking of natural gas: a reaction kinetic approach. *Chem. Geol.* **149**(3–4), 235–250.
- Delaney P. T. (1982) Rapid intrusion of magma into wet rock - groundwater-flow due to pore pressure increases. *J. Geophys. Res.* **87**(NB9), 7739–7756.
- Deyoreo J. J., Lux D. R. and Guidotti C. V. (1991) Thermal modeling in low-pressure high-temperature metamorphic belts. *Tectonophysics* **188**(3–4), 209–238.
- Dickens G. R., Oneil J. R., Rea D. K. and Owen R. M. (1995) Dissociation of oceanic methane hydrate as a cause of the carbon-isotope excursion at the end of the Paleocene. *Paleoceanography* **10**(6), 965–971.
- Dow W. G. (1977) Kerogen studies and geological interpretations. *J. Geochem. Explor.* **7**, 79–99.
- Drits V. A., Lindgreen H., Sakharov B. A., Jakobsen H. J., Fallick A. E., Salyn A. L., Dainyak L. G., Zviagina B. B. and Barfod D. N. (2007) Formation and transformation of mixed-layer minerals by tertiary intrusives in cretaceous mudstones, West Greenland. *Clays Clay Miner.* **55**(3), 260–283.
- Dutrow B. L., Travis B. J., Gable C. W. and Henry D. J. (2001) Coupled heat and silica transport associated with dike intrusion into sedimentary rock: effects on isotherm location and permeability evolution. *Geochim. Cosmochim. Acta* **65**(21), 3749–3767.
- England W. A., Mackenzie A. S., Mann D. M. and Quigley T. M. (1987) The movement and entrapment of petroleum fluids in the subsurface. *J. Geol. Soc. London* **144**, 327–347.
- Falkowski P., Scholes R. J., Boyle E., Canadell J., Canfield D., Elser J., Gruber N., Hibbard K., Hogberg P., Linder S., Mackenzie F. T., Moore, III, B., Pedersen T., Rosenthal Y., Seitzinger S., Smetacek V. and Steffen W. (2000) The global carbon cycle: a test of our knowledge of earth as a system. *Science* **290**(5490), 291–296.
- Faure G. (1986) *Principles of Isotope Geology*, second ed. John Wiley & Sons Inc..
- Faure K. and Cole D. (1999) Geochemical evidence for lacustrine microbial blooms in the vast Permian Main Karoo, Parana, Falkland Islands and Huab basins of southwestern Gondwana. *Palaeogeogr. Palaeoclimatol.* **152**(3–4), 189–213.
- Finkelman R. B., Bostick N. H., Dulong F. T., Senftle F. E. and Thorpe A. N. (1998) Influence of an igneous intrusion on the inorganic geochemistry of a bituminous coal from Pitkin County, Colorado. *Int. J. Coal Geol.* **36**(3–4), 223–241.
- Fjeldskaar W., Helset H. M., Johansen H., Grunnaleiten I. and Horstad I. (2008) Thermal modelling of magmatic intrusions in the Gjallar Ridge, Norwegian Sea: implications for vitrinite reflectance and hydrocarbon maturation. *Basin Res.* **20**(1), 143–159.
- Friedlingstein P., Cox P., Betts R., Bopp L., Von Bloh W., Brovkin V., Cadule P., Doney S., Eby M., Fung I., Bala G., John J., Jones C., Joos F., Kato T., Kawamiya M., Knorr W., Lindsay K., Matthews H. D., Raddatz T., Rayner P., Reick C., Roeckner E., Schnitzler K. G., Schnur R., Strassmann K., Weaver A. J., Yoshikawa C. and Zeng N. (2006) Climate-carbon cycle feedback analysis: results from the (CMIP)-M-4 model intercomparison. *J. Climate* **19**(14), 3337–3353.
- Galushkin Y. I. (1997) Thermal effects of igneous intrusions on maturity of organic matter: a possible mechanism of intrusion. *Org. Geochem.* **26**(11–12), 645–658.
- Ganino C. and Arndt N. T. (2009) Climate changes caused by degassing of sediments during the emplacement of Large Igneous Provinces. *Geology* **37**(4), 323–326.
- George S. C. (1992) Effect of igneous intrusion on the organic geochemistry of a siltstone and an oil shale horizon in the Midland Valley of Scotland. *Org. Geochem.* **18**(5), 705–723.
- Golab A. N. and Carr P. F. (2004) Changes in geochemistry and mineralogy of thermally altered coal, Upper Hunter Valley, Australia. *Int. J. Coal Geol.* **57**(3–4), 197–210.
- Golab A. N., Hutton A. C. and French D. (2007) Petrography, carbonate mineralogy and geochemistry of thermally altered coal in Permian coal measures, Hunter Valley, Australia. *Int. J. Coal Geol.* **70**(1–3), 150–165.
- Grant J. A. (2004) Liquid compositions from low-pressure experimental melting of pelitic rock from Morton Pass, Wyoming, USA. *J. Metamorph. Geol.* **22**(2), 65–78.
- Gregg M. L., Campbell J. H. and Taylor J. R. (1981) Laboratory and modeling investigation of a Colorado oil-shale block heated to 900-degrees-C. *Fuel* **60**(3), 179–188.
- Gröcke D. R., Rimmer S. M., Yoksoulia L. E., Cairncross B., Tsikos H. and van Hunen J. (2009) No evidence for thermogenic methane release in coal from the Karoo-Ferrar Large Igneous Province. *Earth Planet. Sci. Lett.* **277**(1–2), 204–212.
- Gurba L. W. and Weber C. R. (2001) Effects of igneous intrusions on coalbed methane potential, Gunnedah Basin, Australia. *Int. J. Coal Geol.* **46**(2–4), 113–131.
- Hanson R. B. and Barton M. D. (1989) Thermal development of low-pressure metamorphic belts – results from two-dimensional numerical-models. *J. Geophys. Res. Solid* **94**(B8), 10363–10377.
- Hesselbo S. P., Gröcke D. R., Jenkyns H. C., Bjerrum C. J., Farrimond P., Bell H. S. M. and Green O. R. (2000) Massive dissociation of gas hydrate during a Jurassic oceanic anoxic event. *Nature* **406**(6794), 392–395.
- Higgins J. A. and Schrag D. P. (2006) Beyond methane: towards a theory for the Paleocene-Eocene Thermal Maximum. *Earth Planet. Sci. Lett.* **245**(3–4), 523–537.
- Holness M. B. and Isherwood C. E. (2003) The aureole of the Rum Tertiary Igneous Complex, Scotland. *J. Geol. Soc. London* **160**(1), 15–27.
- Holness M. B. and Watt G. R. (2002) The aureole of the Traigh Bhan na Sgurra Sill, Isle of Mull: reaction-driven micro-cracking during pyrometamorphism. *J. Petrol.* **43**(3), 511–534.
- Huff T. A. and Nabelek P. I. (2007) Production of carbonic fluids during metamorphism of graphitic pelites in a collisional orogen – an assessment from fluid inclusions. *Geochim. Cosmochim. Acta* **71**(20), 4997–5015.
- Hunt J. M. (1996) *Petroleum Geochemistry and Geology*, second ed. W.H. Freeman and Company.
- Jaeger J. C. (1959) Temperatures outside a cooling intrusive sheet. *Am. J. Sci.* **257**(1), 44–54.
- Jamtveit B., Buchernurminen K. and Stijfhoorn D. E. (1992) Contact-metamorphism of layered shale carbonate sequences in the Oslo Rift. 1. Buffering, infiltration, and the mechanisms of mass-transport. *J. Petrol.* **33**(2), 377–422.
- Jamtveit B., Svensen H. and Podladchikov Y. Y. (2004) Hydrothermal vent complexes associated with sill intrusions in sedimentary basins. In *Physical Geology of High-level Magmatic Systems*, vol. 234 (eds. C. Breitzkreuz and N. Petford). Geological Society, London, Special Publications, pp. 233–241.
- Jamtveit B. and Yardley B. (1997) *Fluid Flow and Transport in Rocks. Mechanisms and Effects*. Chapman and Hall.
- Jenkyns H. C. (1988) The early Toarcian (Jurassic) anoxic event – stratigraphic, sedimentary, and geochemical evidence. *Am. J. Sci.* **288**(2), 101–151.
- Jenkyns H. C. and Clayton C. J. (1997) Lower Jurassic epicontinental carbonates and mudstones from England and Wales: chemostratigraphic signals and the early Toarcian anoxic event. *Sedimentology* **44**(4), 687–706.
- Karlsen D. A. and Skeie J. E. (2006) Petroleum migration, faults and overpressure. Part I: calibrating basin modelling using petroleum in traps – a review. *J. Petrol. Geol.* **29**(3), 227–255.

- Kerrick D. M. and Caldeira K. (1993) Paleoatmospheric consequences of CO₂ released during early cenozoic regional metamorphism in the Tethyan Orogen. *Chem. Geol.* **108**(1–4), 201–230.
- Kerrick D. M. and Caldeira K. (1998) Metamorphic CO₂ degassing from orogenic belts. *Chem. Geol.* **145**(3–4), 213–232.
- Kjeldstad A., Langtangen H. P., Skogseid J. and Bjørlykke K. (2003) Simulation of Sedimentary Basins. In *Advanced Topics in Computational Partial Differential Equations – Numerical Methods and Diffpack Programming*, vol. 33 (eds. H. P. Langtangen and A. Tveito). Springer Verlag, pp. 611–658.
- Kokelaar B. P. (1982) Fluidization of wet sediments during the emplacement and cooling of various igneous bodies. *J. Geol. Soc. London* **139**(JAN), 21–33.
- Kontorovich A. E., Khomenko A. V., Burshtein L. M., Likhanov I. I., Pavlov A. L., Staroseltsev V. S. and Ten A. A. (1997) Intense basic magmatism in the Tunguska petroleum basin, eastern Siberia, Russia. *Petrol. Geosci.* **3**(4), 359–369.
- Litvinovski B. A., Podladchikov Y. Y., Zanzilevitch A. N. and Dunitchev V. M. (1990) On the melting of acidic volcanites in the contact of basic magma at shallow depth. *Geochimya* **6**, 807–814.
- Lorant F., Prinzhofer A., Behar F. and Huc A.-Y. (1998) Carbon isotopic and molecular constraints on the formation and the expulsion of thermogenic hydrocarbon gases. *Chem. Geol.* **147**(3–4), 249–264.
- Manning C. E. and Bird D. K. (1991) Porosity evolution and fluid-flow in the basalts of the Skaergaard Magma-Hydrothermal System, East Greenland. *Am. J. Sci.* **291**(3), 201–257.
- Mastalerz M., Drobnik A. and Schimmelmann A. (2009) Changes in optical properties, chemistry, and micropore and mesopore characteristics of bituminous coal at the contact with dikes in the Illinois Basin. *Int. J. Coal Geol.* **77**(3–4), 310–319.
- McElwain J. C., Beerling D. J. and Woodward F. I. (1999) Fossil plants and global warming at the Triassic–Jurassic boundary. *Science* **285**(5432), 1386–1390.
- McElwain J. C., Wade-Murphy J. and Hesselbo S. P. (2005) Changes in carbon dioxide during an oceanic anoxic event linked to intrusion into Gondwana coals. *Nature* **435**(7041), 479–482.
- Métrich N. and Rutherford M. J. (1998) Low pressure crystallization paths of H₂O-saturated basaltic–hawaiitic melts from Mt Etna: implications for open-system degassing of basaltic volcanoes. *Geochim. Cosmochim. Acta* **62**(7), 1195–1205.
- Meyers P. A. and Simoneit B. R. T. (1999) Effects of extreme heating on the elemental and isotopic compositions of an Upper Cretaceous coal. *Org. Geochem.* **30**(5), 299–305.
- Mjelde R., Digranes P., Shimamura H., Shiobara H., Kodaira S., Brekke H., Egebjerg T., Sørensen N. and Thorbjørnsen S. (1998) Crustal structure of the northern part of the Vøring Basin, mid-Norway margin, from wide-angle seismic and gravity data. *Tectonophysics* **293**(3–4), 175–205.
- Nabelek P. I. (2007) Fluid evolution and kinetics of metamorphic reactions in calc-silicate contact aureoles – from H₂O to CO₂ and back. *Geology* **35**, 927–930.
- Nichols G. T., Wyllie P. J. and Stern C. R. (1994) Subduction zone melting of pelagic sediments constrained by melting experiments. *Nature* **371**(6500), 785–788.
- Oliver N. H. S., Rubenach M. J., Fu B., Baker T., Blenkinsop T. G., Cleverley J. S., Marshall L. J. and Ridd P. J. (2006) Granite-related overpressure and volatile release in the mid crust: fluidized breccias from the Cloncurry District, Australia. *Geofluids* **6**(4), 346–358.
- Osborne M. J. and Swarbrick R. E. (1997) Mechanisms for generating overpressure in sedimentary basins: a reevaluation. *AAPG Bull.* **81**(6), 1023–1041.
- Othman R., Arouri K. R., Ward C. R. and McKirdy D. M. (2001) Oil generation by igneous intrusions in the northern Gunnedah Basin, Australia. *Org. Geochem.* **32**(10), 1219–1232.
- Pagani M., Caldeira K., Archer D. and Zachos J. C. (2006) Atmosphere: an ancient carbon mystery. *Science* **314**(5805), 1556–1557.
- Panchuk K., Ridgwell A. and Kump L. R. (2008) Sedimentary response to Paleocene-Eocene Thermal Maximum carbon release: a model-data comparison. *Geology* **36**(4), 315–318.
- Pattison D. R. M. (2006) The fate of graphite in prograde metamorphism of pelites: An example from the Ballachulish aureole, Scotland. *Lithos* **88**(1–4), 85–99.
- Payne J. L. and Kump L. R. (2007) Evidence for recurrent Early Triassic massive volcanism from quantitative interpretation of carbon isotope fluctuations. *Earth Planet. Sci. Lett.* **256**(1–2), 264–277.
- Perregaard J. and Schiener E. J. (1979) Thermal alteration of sedimentary organic matter by a basalt intrusive (Kimmeridgian shales, Milne Land, East Greenland). *Chem. Geol.* **26**, 331–343.
- Peters K. E., Walters C. C. and Mankiewicz P. J. (2006) Evaluation of kinetic uncertainty in numerical models of petroleum generation. *AAPG Bull.* **90**(3), 387–403.
- Peters K. E., Whelan J. K., Hunt J. M. and Tarafa M. E. (1983) Programmed pyrolysis of organic matter from thermally altered Cretaceous black shales. *AAPG Bull.* **67**(11), 2137–2146.
- Planke S., Rassmussen T., Rey S. S. and Myklebust R. (2005) Seismic characteristics and distribution of volcanic intrusions and hydrothermal vent complexes in the Vøring and Møre basins. In *Petroleum Geology: North-West Europe and Global Perspectives* (eds. A. Dore and B. Vining). The Geological Society London.
- Podladchikov Y. Y. and Wickham S. M. (1994) Crystallization of hydrous magmas – calculation of associated thermal effects, volatile fluxes, and isotopic alteration. *J. Geol.* **102**(1), 25–45.
- Polteau S., Mazzini A., Galland O., Planke S. and Malthe-Sørensen A. (2008) Saucer-shaped intrusions: occurrences, emplacement and implications. *Earth Planet. Sci. Lett.* **266**(1–2), 195–204.
- Polyansky O. P. and Reverdatto V. V. (2006) Contact metamorphism and metasomatism near the Talnakh intrusion: fluid convection and heat transfer modeling on the basis of the finite-difference method. *Dokl. Earth Sci.* **114**(9), 803–807.
- Powers S. and Clapp F. G. (1932) Nature and origin of occurrences of oil, gas, and Bitumen in igneous and metamorphic rocks. *AAPG Bull.* **16**(8), 719–726.
- Raymond A. C. and Murchison D. G. (1988) Development of organic maturation in the thermal aureoles of sills and its relation to sediment compaction. *Fuel* **67**(12), 1599–1608.
- Reiter M. and Tovar R. J. C. (1982) Estimates of terrestrial heat-flow in Northern Chihuahua, Mexico, based upon petroleum bottom-hole temperatures. *Geol. Soc. Am. Bull.* **93**(7), 613–624.
- Retallack G. and Jahren A. H. (2008) Methane release from igneous intrusion of coal during late Permian extinction events. *J. Geol.* **116**(1), 1–20.
- Reverdatto V. V. and Melenevskii V. N. (1983) Magmatic heat as a factor in generation of hydrocarbons: the case of basalt sills. *Geol. Geofiz.* **24**(6), 15–23.
- Ripley E. M. and Taib N. I. (1989) Carbon isotopic studies of metasedimentary and igneous rocks at the Babbitt Cu–Ni deposit, Duluth complex, Minnesota, USA. *Chem. Geol.* **73**(4), 319–342.
- Rodriguez Monreal F., Villar H. J., Baudino R., Delpino D. and Zencich S. (2009) Modeling an atypical petroleum system: a case study of hydrocarbon generation, migration and accumu-

- lation related to igneous intrusions in the Neuquen Basin, Argentina. *Mar. Petrol. Geol.* **26**(4), 590–605.
- Saghafi A., Faiz M. and Roberts D. (2007) CO₂ storage and gas diffusivity properties of coals from Sydney Basin, Australia. *Int. J. Coal Geol.* **70**(1–3), 240–254.
- Saghafi A., Pinetown K. L., Grobler P. G. and van Heerden J. H. P. (2008) CO₂ storage potential of South African coals and gas entrapment enhancement due to igneous intrusions. *Int. J. Coal Geol.* **73**(1), 74–87.
- Santos R. V., Dantas E. L., Oliveira C. G. d., Alvarenga C. J. S. d., Anjos C. W. D. d., Guimarães E. M. and Oliveira F. B. (2009) Geochemical and thermal effects of a basic sill on black shales and limestones of the Permian Irati Formation. *J. S. Am. Earth Sci.* **28**(1), 14–24.
- Saxby J. D. and Stephenson L. C. (1987) Effect of an igneous intrusion on oil shale at Rundle (Australia). *Chem. Geol.* **63**(1–2), 1–16.
- Schenk H. J., DiPrimio R. and Horsfield B. (1997) The conversion of oil into gas in petroleum reservoirs. 1. Comparative kinetic investigation of gas generation from crude oils of lacustrine, marine and fluviodeltaic origin by programmed-temperature closed-system pyrolysis. *Org. Geochem.* **26**(7–8), 467–481.
- Schimmelmann A., Mastalerz M., Gao L., Sauer P. E. and Topalov K. (2009) Dike intrusions into bituminous coal, Illinois Basin: H, C, N, O isotopic responses to rapid and brief heating. *Geochim. Cosmochim. Acta* **73**(20), 6264–6281.
- Shih S.-M. and Sohn H. Y. (1978) A mathematical model for the retorting of a large block of oil shale: effect of the internal temperature gradient. *Fuel* **57**(10), 622–630.
- Simoneit B. R. T., Brenner S., Peters K. E. and Kaplan I. R. (1978) Thermal alteration of cretaceous Black Shale by basaltic intrusions in Eastern Atlantic. *Nature* **273**(5663), 501–504.
- Simoneit B. R. T., Brenner S., Peters K. E. and Kaplan I. R. (1981) Thermal alteration of cretaceous Black Shale by diabase intrusions in the Eastern Atlantic. 2. Effects on Bitumen and Kerogen. *Geochim. Cosmochim. Acta* **45**(9), 1581–1602.
- Skinner E. M. W. and Marsh J. S. (2004) Distinct kimberlite pipe classes with contrasting eruption processes. *Lithos* **76**(1–4), 183–200.
- Snowdon L. R. (1979) Errors in extrapolation of experimental kinetic parameters to organic geochemical systems. *AAPG Bull.* **63**(7), 1128–1134.
- Snyman C. P. and Barclay J. (1989) The coalification of South-African coal. *Int. J. Coal Geol.* **13**(1–4), 375–390.
- Storey M., Duncan R. A. and Swisher, III, C. C. (2007) Paleocene-Eocene Thermal Maximum and the opening of the Northeast Atlantic. *Science* **316**(5824), 587–589.
- Storvoll V., Bjørlykke K. and Mondol N. H. (2005) Velocity-depth trends in mesozoic and cenozoic sediments from the Norwegian shelf. *AAPG Bull.* **89**(3), 359–381.
- Stothers R. B. (1993) Flood basalts and extinction events. *Geophys. Res. Lett.* **20**(13), 1399–1402.
- Svensen H., Bebout G., Kronz A., Li L., Planke S., Chevallier L. and Jamtveit B. (2008) Nitrogen geochemistry as a tracer of fluid flow in a hydrothermal vent complex in the Karoo Basin, South Africa. *Geochim. Cosmochim. Acta* **72**(20), 4929–4947.
- Svensen H. and Jamtveit B. (1998) Contact metamorphism of shales and limestones from the Grua area, the Oslo Rift, Norway: a phase-petrological study. *Norsk Geol. Tidssk.* **78**, 81–98.
- Svensen H., Jamtveit B., Planke S. and Chevallier L. (2006) Structure and evolution of hydrothermal vent complexes in the Karoo Basin, South Africa. *J. Geol. Soc. London* **163**(4), 671–682.
- Svensen H., Planke S., Chevallier L., Malthé-Sorensen A., Corfu F. and Jamtveit B. (2007) Hydrothermal venting of greenhouse gases triggering Early Jurassic global warming. *Earth Planet. Sci. Lett.* **256**(3–4), 554–566.
- Svensen H., Planke S. and Corfu F. (2010) Zircon dating ties NE Atlantic sill emplacement to initial Eocene global warming. *J. Geol. Soc. London* **167**(3), 433–436.
- Svensen H., Planke S., Malthé-Sorensen A., Jamtveit B., Myklebust R., Eidem T. R. and Rey S. S. (2004) Release of methane from a volcanic basin as a mechanism for initial Eocene global warming. *Nature* **429**(6991), 542–545.
- Svensen H., Planke S., Polozov A. G., Schmidbauer N., Corfu F., Podladchikov Y. Y. and Jamtveit B. (2009) Siberian gas venting and the end-Permian environmental crisis. *Earth Planet. Sci. Lett.* **277**(3–4), 490–500.
- Sweeney J. and Burnham A. K. (1990) Evaluation of a simple model of vitrinite reflectance based on chemical kinetics. *AAPG Bull.* **74**(10), 1559–1570.
- Tingay M. R. P., Hillis R. R., Swarbrick R. E., Morley C. K. and Damit A. R. (2009) Origin of overpressure and pore-pressure prediction in the Baram province, Brunei. *AAPG Bull.* **93**(1), 51–74.
- Tissot B. and Welte D. H. (1984) *Petroleum Formation and Occurrence*. Springer Verlag.
- Tissot B. P., Pelet R. and Ungerer P. (1987) Thermal history of sedimentary basins, maturation indexes, and kinetics of oil and gas generation. *AAPG Bull.* **71**(12), 1445–1466.
- Trommsdorff V. and Connolly J. A. D. (1996) The ultramafic contact aureole about the Bregaglia (Bergell) tonalite: Isograds and a thermal model. *Schweiz. Mineral. Petrogr. Mitt.* **76**(3), 537–547.
- Turcotte D. and Schubert G. (2002) *Geodynamics*. Cambridge.
- Ungerer P. and Pelet R. (1987) Extrapolation of the kinetics of oil and gas-formation from laboratory experiments to sedimentary basins. *Nature* **327**(6117), 52–54.
- Visscher H., Looy C. V., Collinson M. E., Brinkhuis H., van Konijnenburg-van Cittert J. H. A., Kärchner W. M. and Septhorn M. A. (2004) Environmental mutagenesis during the end-Permian ecological crisis. *Proc. Natl. Acad. Sci. USA* **101**(35), 12952–12956.
- Wagner W. and Pruss A. (2002) The IAPWS formulation 1995 for the thermodynamic properties of ordinary water substance for general and scientific use. *J. Phys. Chem. Ref. Data* **31**(2), 387–535.
- Walther J. V. and Orville P. M. (1982) Volatile production and transport in regional metamorphism. *Contrib. Mineral. Petrol.* **79**(3), 252–257.
- Walther J. V. and Wood B. J. (1984) Rate and mechanism in prograde metamorphism. *Contrib. Mineral. Petrol.* **88**(3), 246–259.
- Whiticar M. J. (1996) Stable isotope geochemistry of coals, humic kerogens and related natural gases. *Int. J. Coal Geol.* **32**(1–4), 191–215.
- Wignall P. B. (2001) Large Igneous Provinces and mass extinctions. *Earth Sci. Rev.* **53**(1–2), 1–33.
- Zhou M. F., Malpas J., Song X. Y., Robinson P. T., Sun M., Kennedy A. K., Leshar C. M. and Keays R. R. (2002) A temporal link between the Emeishan Large Igneous Province (SW China) and the end-Guadalupian mass extinction. *Earth Planet. Sci. Lett.* **196**(3–4), 113–122.
- Zhu D., Jin Z., Hu W., Song Y. and Gao X. (2007) Effect of igneous activity on hydrocarbon source rocks in Jiyang sub-basin, eastern China. *J. Petrol. Sci. Eng.* **59**(3–4), 309–320.